Commun. Comput. Phys.
doi: 10.4208/cicp.050610.021210a

Vol. **10**, No. 5, pp. 1161-1183
November 2011

Split Local Artificial Boundary Conditions for the Two-Dimensional Sine-Gordon Equation on $\mathbb{R}^2$

Houde Han* and Zhiwen Zhang

Department of Mathematical Sciences, Tsinghua University, Beijing 100084, China.

Received 5 June 2010; Accepted (in revised version) 2 December 2010

Available online 2 August 2011

Abstract. In this paper the numerical solution of the two-dimensional sine-Gordon equation is studied. Split local artificial boundary conditions are obtained by the operator splitting method. Then the original problem is reduced to an initial boundary value problem on a bounded computational domain, which can be solved by the finite difference method. Several numerical examples are provided to demonstrate the effectiveness and accuracy of the proposed method, and some interesting propagation and collision behaviors of the solitary wave solutions are observed.

AMS subject classifications: 52B10, 65D18, 68U05, 68U07

Key words: Sine-Gordon equation, operator splitting method, artificial boundary condition, soliton, unbounded domain.

1 Introduction

The sine-Gordon equation is a nonlinear hyperbolic partial differential equation, which was originally considered in the nineteenth century in the course of study of surfaces of constant negative curvature. Then it attracted a lot of attention in the 1970s due to the presence of soliton solutions. In recent years the sine-Gordon equation has also been used to describe physical models which possess soliton-like structures in higher dimensions. A typical example is the Josephson junction model which consists of two layers of super conducting material separated by an isolating barrier [1, 2]. This paper is devoted to study the numerical solution of the two-dimensional sine-Gordon equation on $\mathbb{R}^2$.

The initial value problem of the two-dimensional sine-Gordon equation is given by the following problem:

$$\frac{\partial^2 u}{\partial t^2}-\frac{\partial^2 u}{\partial x^2}-\frac{\partial^2 u}{\partial y^2}+\sin(u)=0, \quad x,y\in\mathbb{R}^1, \quad t>0, \tag{1.1a}$$

*Corresponding author. *Email addresses:* `hhan@math.tsinghua.edu.cn` (H. Han), `zhangzhiwen02@mails.tsinghua.edu.cn` (Z. Zhang)

$$u|_{t=0}=\varphi_0(x,y), \quad u_t|_{t=0}=\varphi_1(x,y), \quad x,y\in \mathrm{R}^1, \tag{1.1b}$$

where $u=u(x,y,t)$ represents the wave displacement at position (x,y) and at time t, $\varphi_0(x,y)$, $\varphi_1(x,y)$ are the initial displacement and velocity respectively, and $\sin(u)$ is the nonlinear force term.

The essential difficulty of the numerical solution to the problem (1.1a)-(1.1b) involves two parts, the nonlinearity of the equation and the unboundedness of the physical domain. For the bounded domain case, there are a lot of studies on the numerical solution of the two-dimensional sine-Gordon equation with Dirichlet, Neumann or periodic boundary condition. For example, Guo et al. [5] used finite difference scheme to investigate the numerical solution of the sine-Gordon equation with periodic boundary condition. Xin [6] studied the sine-Gordon equation as an asymptotic reduction of the two level dissipationless Maxwell-Bloch system. In addition, Christiansen and Lomdahl [7] used a generalized leap frog method, Argyris et al. [8] used a finite element approach, Sheng et al. [9] adopted a split cosine scheme, Djidjeli et al. [10] used a two-step one-parameter leapfrog scheme, A. G. Bratsos [11] used a three time-level fourth-order explicit finite-difference scheme, to simulate the sine-Gordon equation. Recently, A. G. Bratsos [12] adopted the method of lines to solve the two-dimensional sine-Gordon equation. M. Dehghan and A. Shokri [13] used the radial basis functions to solve the two-dimensional sine-Gordon equation. D. Mirzaei and M. Dehghan [14] used the continuous linear elements to obtain the boundary element solution of the two-dimensional sine-Gordon equation. However, when one wants to solve the two-dimensional sine-Gordon equation on the unbounded domain, these methods will face essential difficulties. Since the unboundedness of the physical domain in the problem (1.1a)-(1.1b), the standard finite element method or finite difference method cannot be used directly. In this paper, we will consider the numerical solution of the two-dimensional sine-Gordon equation on the unbounded domain.

The artificial boundary condition (ABC) method is a powerful approach to reduce the problems on the unbounded domain to a bounded computational domain. In general, the artificial boundary conditions can be classified into implicit boundary conditions and explicit boundary conditions including global, also called nonlocal ABC, local ABC and discrete ABC [4]. For the last thirty years, many mathematicians have made great contributions on this subject, see [15–19], which makes the artificial boundary condition method for the linear partial differential equations on the unbounded domain become a well developed method. In recent few years, there have been some new progress on the artificial boundary condition method for nonlinear partial differential equations on the unbounded domain. H. Han et al. [20] and Z. Xu et al. [21] used the Cole-Hopf transformation to get the exact ABCs for the viscous Burger's equation and the deterministic KPZ equation. Zheng [23, 24] adopted the inverse scattering approach to obtain the exact ABCs for the one-dimensional cubic nonlinear Schrödinger equation and the one-dimensional sine-Gordon equation. H. Han et al. [22] also utilized an operator splitting method to design split local artificial boundary conditions for the one-dimensional nonlinear Klein-Gordon equations.

In this paper, we use the operator splitting method to obtain the split local artificial boundary conditions for the two-dimensional sine-Gordon equation on R^2. Then reduce the original problem (1.1a)-(1.1b) into an initial boundary value problem on a bounded computational domain, which can be solved by the finite difference method.

The organization of this paper is as follows: in Section 2, we propose a split local artificial boundary condition for the two-dimensional sine-Gordon equation on R^2 based on the operator splitting method. A finite difference scheme is given by the coupling procedure in Section 3. In Section 4, we give some numerical examples to test the convergence and accuracy of the proposed method. We make some concluding remarks in Section 5.

2 The split local artificial boundary method

2.1 The operator splitting method

The operator splitting method [29, 30] is a powerful approach for numerical simulation of complex physical time-dependent models, where the simultaneous effect of several different subprocess has to be considered. Mathematical models of such phenomena are usually described by time-dependent partial differential equations, which include several spatial differential operators. Each of them is corresponding to a subprocess of the physical phenomenon. Generally speaking, every subprocess is simpler than the whole spatial differential operator.

In [22], Han et al. proposed a split local absorbing conditions for the one-dimensional nonlinear Klein-Gordon equation on R^1. The basic idea is using the operator splitting method on the boundaries to construct boundary conditions. In this paper, we extend this idea to construct the artificial boundary conditions for the two-dimensional sine-Gordon problem (1.1a)-(1.1b) on R^2.

For Eq. (1.1a), we introduce an auxiliary function $v=u_t$, and denote the vector function $U=[u,v]^T$. Then Eq. (1.1a) can be converted into a differential equation system:

$$U_t=\begin{pmatrix} u \\ v \end{pmatrix}_t=\begin{pmatrix} v \\ u_{xx}+u_{yy}-\sin(u) \end{pmatrix}. \tag{2.1}$$

We introduce a splitting control parameter $\alpha\in(0,1)$, the previous two-dimensional sine-Gordon problem (1.1a)-(1.1b) can be written in a splitting form.

$$U_t=\begin{pmatrix} u \\ v \end{pmatrix}_t=\begin{pmatrix} \alpha^2 v \\ u_{xx}+u_{yy} \end{pmatrix}+\begin{pmatrix} (1-\alpha^2)v \\ -\sin(u) \end{pmatrix}:=\mathcal{L}_1 U+\mathcal{L}_2(U), \tag{2.2a}$$

$$U|_{t=0}=\begin{pmatrix} \varphi_0(x,y) \\ \varphi_1(x,y) \end{pmatrix}. \tag{2.2b}$$

From time $t=t_n$ to time $t=t_{n+1}$, where $t_{n+1}=t_n+\tau$, $t^0=0$, we assume the solution

$$U(x,y,t_n)=\big[u(x,y,t_n),v(x,y,t_n)\big]^T$$

is given. Then we solve Eq. (2.2a) with the initial condition $U(x,y,t_n)$ in a small time step τ to obtain $U(x,y,t_{n+1})$. First of all, we split the problem with Eq. (2.2a) and the initial condition $U(x,y,t_n)$ into a linear subproblem

$$U_t^1 = \mathcal{L}_1 U^1, \quad x,y \in \mathbb{R}^1, \quad t \in [t_n, t_{n+1}], \tag{2.3a}$$
$$U^1(x,y,t_n) = U(x,y,t_n), \tag{2.3b}$$

and a nonlinear subproblem

$$U_t^2 = \mathcal{L}_2(U^2), \quad x,y \in \mathbb{R}^1, \quad t \in [t_n, t_{n+1}], \tag{2.4a}$$
$$U^2(x,y,t_n) = U^1(x,y,t_{n+1}). \tag{2.4b}$$

Then we solve the subproblems (2.3a)-(2.3b) and (2.4a)-(2.4b) step by step, in which the solution of one subproblem is employed as the initial condition for the alternative subproblem, and take

$$U(x,y,t_{n+1}) \approx U^2(x,y,t_{n+1})$$

as the approximate solution to the problem (1.1a)-(1.1b) at time $t = t_{n+1}$. More precisely, let us define the flow map $\mathcal{F}_1^\tau$ associated with the solution of the subproblem (2.3a)-(2.3b) by

$$\mathcal{F}_1^\tau \big(U^1(x,y,t_n) \big) = U^1(x,y,t_{n+1})$$

and the flow map $\mathcal{F}_2^\tau$ associated with the solution of the subproblem (2.4a)-(2.4b) by

$$\mathcal{F}_2^\tau (U^2(x,y,t_n)) = U^2(x,y,t_{n+1}).$$

Then the first-order approximation solution can be written in a compact form:

$$U^{n+1} \approx \mathcal{F}_2^\tau \circ \mathcal{F}_1^\tau (U^n) := \mathcal{F}_2^\tau \big(\mathcal{F}_1^\tau (U^n) \big). \tag{2.5}$$

So far, the simplest idea of the operator splitting method has been described. The error of the approximation (2.5) is the first-order $\mathcal{O}(\tau)$ induced by the noncommutativity of the operators $\mathcal{L}_1$ and $\mathcal{L}_2$. In general, the Strang splitting [29] is more frequently adopted in applications, for which the approximation solution is approximated by,

$$U^{n+1} \approx \mathcal{F}_2^{\frac{\tau}{2}} \circ \mathcal{F}_1^\tau \circ \mathcal{F}_2^{\frac{\tau}{2}} (U^n). \tag{2.6}$$

In practical computation, the only difference between the Strang splitting method [29] and the first-order splitting method is that the first and last steps are half of the normal step τ.

2.2 Construct the split local ABC

In this section, we discuss the split local artificial boundary condition for the two-dimensional sine-Gordon problem (1.1a)-(1.1b) on R^2. Simple calculation shows that the equation of the linear subproblem (2.3a)-(2.3b) is equivalent to the following wave equation:

$$u_{tt}-\alpha^2 u_{xx}-\alpha^2 u_{yy}=0, \quad x,y\in R^1, \quad t>0. \tag{2.7}$$

Notice that the equation of the nonlinear subproblem (2.4a)-(2.4b) is a first order ordinary differential equation system, in which only the time derivative involved, hence no extra boundary condition is required.

Next we consider how to obtain the local artificial boundary condition for the wave equation (2.7). First of all, we introduce four artificial boundaries,

$$\begin{aligned}
&\Sigma_e=\big\{(x,y,t)|x=x_e, \quad y_s\le y\le y_n, \quad 0\le t\le T\big\},\\
&\Sigma_w=\big\{(x,y,t)|x=x_w, \quad y_s\le y\le y_n, \quad 0\le t\le T\big\},\\
&\Sigma_n=\big\{(x,y,t)|x_w\le x\le x_e, \quad y=y_n, \quad 0\le t\le T\big\},\\
&\Sigma_s=\big\{(x,y,t)|x_w\le x\le x_e, \quad y=y_s, \quad 0\le t\le T\big\},
\end{aligned}$$

where x_w, x_e, y_s, y_n are four constants, with $x_w<x_e$ and $y_s<y_n$, which divide the unbounded domain $R^2\times[0,T]$ into a bounded domain D_i and an unbounded domain D_e, namely,

$$\begin{aligned}
&D_i=\big\{(x,y,t)|x_w<x<x_e, \quad y_s<y<y_n, \quad 0\le t\le T\big\},\\
&D_e=R^2\times[0,T]\setminus\overline{D_i},
\end{aligned}$$

where $\overline{D_i}$ denotes the closure of the set D_i. The bounded domain D_i is the computational domain. We must find some appropriate boundary conditions on Σ_e, Σ_w, Σ_n and Σ_s, respectively, to reduce the original linear subproblem (2.3a)-(2.3b) into an initial boundary value problem on the bounded domain D_i.

In order to limit the scope of this paper somewhat, we assume that during the whole propagation process *only the waves in the interior domain will move out of the domain D_i through the artificial boundaries and there will be no waves traveling from the exterior domain into the interior domain D_i*. That means the local artificial boundary conditions are transparent for the out-going waves.

Next, one consider a plane wave solution to Eq. (2.7) of the following form,

$$u(x,y,t)=e^{-i(\omega t-\xi x-\eta y)}, \tag{2.8}$$

where ω is the time frequency, ξ and η are the wave numbers in x- and y-directions respectively. We have the dual relation between the space-time domain (x,y,t) and the wave number-frequency domain

$$(\xi,\eta,\omega):\ \xi\leftrightarrow -i\frac{\partial}{\partial x}, \quad \eta\leftrightarrow -i\frac{\partial}{\partial y} \quad \text{and} \quad \omega\leftrightarrow i\frac{\partial}{\partial t}.$$

Apply the ansatz (2.8) to Eq. (2.7), one obtains the corresponding *dispersion relation*,

$$\omega^2=\alpha^2(\xi^2+\eta^2). \tag{2.9}$$

For the sake of simplicity, we discuss the local artificial boundary condition *on the east boundary* Σ_e. Under the framework of Engquist and Majda's pseudo-differential operator approach, see [15, 25], the exact artificial boundary condition on the east boundary Σ_e is obtained by solving the dispersion equation (2.9) to get an expression for the wave number ξ, namely,

$$\alpha\xi=\pm\omega\sqrt{1-\frac{\alpha^2\eta^2}{\omega^2}}. \tag{2.10}$$

We assume the time frequency ω and the wave number ξ are both positive numbers. Under this assumption, the positive and negative signs in Eq. (2.10) correspond to the right-going and left-going waves, respectively. According to our assumption, the waves will move out of the domain D_i through the east boundary Σ_e and no waves travel from the exterior domain into the interior domain D_i, namely, there are only right-going waves on the east boundary Σ_e. Therefore we drop the negative sign in the dispersion relation (2.10) and obtain,

$$\alpha\xi=\omega\sqrt{1-\frac{\alpha^2\eta^2}{\omega^2}}. \tag{2.11}$$

The exact artificial boundary condition can be obtained by transforming the dispersion equation (2.11) into the space-time domain (x,y,t). The result is a pseudo-differential equation applied to the boundary Σ_e, which can perfectly absorb all the right-going waves impinging on the boundary Σ_e. However, the pseudo-differential form of the artificial boundary condition is non-local and does not work for an operator splitting scheme because it is with a memory term in time. In [15,25–27], the authors adopted local approximations to the dispersion equation (2.11) by expanding the square root term to various orders of accuracy. Then they obtained the corresponding local artificial boundary conditions by transforming the approximate dispersion relation into the space-time domain. For example, using the zero order Taylor approximation,

$$\sqrt{1-\frac{\alpha^2\eta^2}{\omega^2}}\approx 1+\mathcal{O}\Big(\frac{\alpha^2\eta^2}{\omega^2}\Big), \tag{2.12}$$

for the square root term in the dispersion equation (2.11) and transforming the approximate dispersion relation into the space-time domain, one obtains

$$\Big(\frac{\partial}{\partial t}+\alpha\frac{\partial}{\partial x}\Big)u|_{\Sigma_e}=0. \tag{2.13}$$

We point out that the approximation (2.12) is called *paraxial approximation* in the literature, which means that the ratio of the time frequency and the wave number in y-direction η/ω

is small. In [22], we indicated that for the one-dimensional wave equation the artificial boundary condition (2.13) is exact. For two-dimensional wave equation, the artificial boundary condition (2.13) is exact only for the waves impinging into the boundary Σ_e in the normal direction. Therefore, one need more accurate approximation to the dispersion equation (2.11) to construct local artificial boundary condition.

In [26,27], the author showed that the differential operators in the space-time domain corresponding to the higher order approximations to the dispersion relation (2.11) can be expressed in the following form

$$\prod_{l=1}^{p}\Big(\cos(\theta_l)\frac{\partial}{\partial t}+\alpha\frac{\partial}{\partial x}\Big)u\Big|_{\Sigma_e}=0, \tag{2.14}$$

where p is an integer and θ_l, $l=1,\cdots,p$ are angles between the wave incident direction and the normal direction of the boundary Σ_e. By the same technique, the local artificial boundary conditions on the west boundary Σ_w, north boundary Σ_n and south boundary Σ_s can be obtained,respectively, which are the following forms,

$$\prod_{l=1}^{p}\Big(\cos(\theta_l)\frac{\partial}{\partial t}-\alpha\frac{\partial}{\partial x}\Big)u\Big|_{\Sigma_w}=0, \tag{2.15a}$$

$$\prod_{l=1}^{p}\Big(\cos(\theta_l)\frac{\partial}{\partial t}+\alpha\frac{\partial}{\partial y}\Big)u\Big|_{\Sigma_n}=0, \tag{2.15b}$$

$$\prod_{l=1}^{p}\Big(\cos(\theta_l)\frac{\partial}{\partial t}-\alpha\frac{\partial}{\partial y}\Big)u\Big|_{\Sigma_s}=0. \tag{2.15c}$$

So far, we have obtained local artificial boundary conditions for Eq. (2.7) on the boundaries Σ_e, Σ_w, Σ_n and Σ_s, respectively. Therefore we can reduce the linear subproblem (2.3a)-(2.3b) into an initial boundary value problem on the bounded computational domain D_i.

The equation of the nonlinear subproblem (2.4a)-(2.4b) is equivalent to the following ordinary differential equation,

$$u_{tt}+(1-\alpha^2)\sin(u)=0,\quad x,y\in\mathrm{R}^1,\quad t>0. \tag{2.16}$$

Note that the restriction of ODE system (2.16) on the bounded computational domain D_i is an initial value problem, which can be solved by the Runge-Kutta method or the Matlab ode-solver (ode15). Therefore, no extra boundary condition is required.

It should be pointed out that the proposed artificial boundary conditions (2.14)-(2.15c) are valid under the conditions that during the whole propagation process only the waves in the interior domain will move out of the domain D_i through the artificial boundaries and there will have no waves traveling from the exterior domain into the interior domain D_i.

3 The derivation of the difference scheme

In this section, we consider the coupling procedure for solving the two-dimensional sine-Gordon problem (1.1a)-(1.1b) on the bounded computational domain $D_i=(x_w,x_e)\times(y_s,y_n)\times[0,T]$. We divide the domain D_i by a set of lines parallel to the x-, y- and t-axis to form a grid, and choose $h_x=(x_r-x_l)/J$, $h_y=(y_t-y_b)/K$ and $\tau=T/N$ for the line spacings, where J, K and N are three positive integers. For simplicity, we assume $h=h_x=h_y$. The *grid points* are given by

$$\Omega=\Big\{(x_j,y_k,t_n)|x_j=x_l+jh,\ y_k=y_b+kh,\ t_n=n\tau,\ j=0,\cdots,J,\ k=0,\cdots,K,\ n=0,\cdots,N\Big\}.$$

Let I_e denote the index set corresponding to the grid points on the east boundary of the bounded domain D_i, that is,

$$I_e=\big\{(j,k)|j=J,\quad 1\le k\le K-1\big\}.$$

Similarly one defines the index sets I_w, I_n and I_s corresponding to the grid points on the west, north and south boundaries of the bounded domain D_i, respectively, as following,

$$\begin{aligned}
&I_w=\big\{(j,k)|j=0,\quad 1\le k\le K-1\big\},\\
&I_n=\big\{(j,k)|k=K,\quad 0\le j\le J\big\},\\
&I_s=\big\{(j,k)|k=0,\quad 0\le k\le J\big\}.
\end{aligned}$$

The indices of the four *corner points* belong to the sets I_n and I_s, which means the numerical solutions on the corner points will be updated by the boundary conditions (2.15b) and (2.15c). Finally, let

$$I_B=I_e\bigcup I_w\bigcup I_n\bigcup I_s$$

denote the index set corresponding to all the grid points on the boundaries of the bounded domain D_i.

Suppose the numerical solutions $\mathbf{u}^n=\{u_{jk}^n|0\le j\le J,\ 0\le k\le K,\ 0\le n\le N\}$ are given at time $t=t_n$, where u_{jk}^n represents the approximation solution of wave displacement $u(x,y,t)$ on the grid point (x_j,y_k,t_n). Let $\mathbf{u}_I^{n+1}=\{u_{jk}^{n+1}|1\le j\le J-1,\ 1\le k\le K-1\}$ denote the numerical solutions in the interior domain D_i and $\mathbf{u}_B^{n+1}=\mathbf{u}^{n+1}\setminus\mathbf{u}_I^{n+1}$ denote the numerical solutions on the boundaries of the domain D_i.

Moveover, one needs to record the values of the auxiliary function $v=u_t$ on the boundaries, namely, assume the numerical solutions $\mathbf{v}_B^n=\{v_{jk}^n|(i,k)\in I_B\}$ are known at time $t=t_n$, where v_{jk}^n represents the approximation solution of the auxiliary function $v(x,y,t)$ on the grid point (x_j,y_k,t_n).

From time $t=t_n$ to time $t=t_{n+1}$, where $t_{n+1}=t_n+\tau$, $t_0=0$, we first use the central difference scheme to discretize Eq. (2.7) at points (x_j,y_k,t_n), $1\le j\le J-1$, $1\le k\le K-1$ in the interior domain D_i and obtain,

$$D_t^+D_t^-u_{jk}^n-\alpha^2D_x^+D_x^-u_{jk}^n-\alpha^2D_y^+D_y^-u_{jk}^n+\sin u_{jk}^n=0,\quad 1\le j\le J-1,\quad 1\le k\le K-1,\qquad (3.1)$$

where $D_\bullet^+$ and $D_\bullet^-$ represent the forward and backward differences in t-, x- or y- direction, respectively. At time $t=t_{n+1}$, we need to obtain the numerical solution $\mathbf{u}^{n+1}$, which contains $(J+1)(K+1)$ unknowns. However the linear equation system (3.1) only has $(J-1)(K-1)$ equations. Therefore we can only get the numerical solutions at time $t=t_{n+1}$ in the interior domain D_i, namely $\mathbf{u}_I^{n+1}$. Thus the $2J+2K$ extra unknown values $\mathbf{u}_B^{n+1}$ must be updated through boundary conditions (2.14)-(2.15c) and (2.16).

We illustrate how to discretize Eq. (2.14) on the artificial boundary Σ_e. Recall that the boundary condition (2.14) on Σ_e is a composition of factors of the form $\cos(\theta_j)\partial/\partial t+\alpha\partial/\partial x$, which can be discretized by $\cos(\theta_j)S_x^-D_t^-+\alpha S_t^-D_x^-$. Here $S_\bullet^-$ denotes the backward sum, namely,

$$S_x^-u_{jk}^n=\frac{u_{j-1,k}^n+u_{jk}^n}{2}\quad\text{and}\quad S_t^-u_{jk}^{n+1}=\frac{u_{jk}^n+u_{jk}^{n+1}}{2}.$$

Hence the boundary condition (2.14) on Σ_e can be discretized by,

$$\Sigma_e:\ \prod_{l=1}^{p}\big(\cos(\theta_l)S_x^-D_t^-+\alpha S_t^-D_x^-\big)u_{J,k}^{n+1}=0,\quad 1\le k\le K-1.\qquad (3.2)$$

Similarly, the boundary conditions on other sides can be discretized by,

$$\Sigma_w:\ \prod_{l=1}^{p}\big(\cos(\theta_l)S_x^+D_t^--\alpha S_t^-D_x^+\big)u_{0,k}^{n+1}=0,\quad 1\le k\le K-1,\qquad (3.3a)$$

$$\Sigma_n:\ \prod_{l=1}^{p}\big(\cos(\theta_l)S_y^-D_t^-+\alpha S_t^-D_y^-\big)u_{j,K}^{n+1}=0,\quad 0\le j\le J,\qquad (3.3b)$$

$$\Sigma_s:\ \prod_{l=1}^{p}\big(\cos(\theta_l)S_y^+D_t^--\alpha S_t^-D_y^+\big)u_{j,0}^{n+1}=0,\quad 0\le j\le J.\qquad (3.3c)$$

Here $S_\bullet^+$ denotes the forward sum, for example, $S_x^+u_{jk}^n=(u_{jk}^n+u_{j+1,k}^n)/2$.

According to the discussion in Section 2, we split the problem (1.1a)-(1.1b) into a linear subproblem (2.3a)-(2.3b) and a nonlinear subproblem (2.4a)-(2.4b) *on the boundaries* of the bounded domain D_i and then solve them separately, in which the solution of one subproblem is employed as an initial condition for the alternative subproblem. For notation convenience, we introduce the intermediate variable $U^*=\{[u_{jk}^*,v_{jk}^*]^T|(i,k)\in I_B\}$.

The restriction of the nonlinear subproblem (2.4a)-(2.4b) on the boundaries is an initial value problem, hence no extra boundary condition is required. We use the flow map operator form to denote the solution after one time step τ, that is,

$$U^* \approx \mathcal{F}_2^{\tau}(U_B^n), \quad (j,k) \in I_B, \tag{3.4}$$

where $U_B^n = [\mathbf{u}_B^n, \mathbf{v}_B^n]^T$. Then we set $v_{jk}^{n+1} = v_{jk}^*$, $(j,k) \in I_B$. Recall that the boundary conditions (2.14)-(2.15c) are obtained from the linear subproblem (2.3a)-(2.3b), hence the solution of the nonlinear subproblem (2.4a)-(2.4b) $u_{jk}^*, (j,k) \in I_B$ will be regarded as the initial data for the subproblem (2.3a)-(2.3b). More precisely, we will replace u_{jk}^n by u_{jk}^*, $(j,k) \in I_B$ and solve Eqs. (3.2)-(3.3c) to obtain the numerical solutions $\mathbf{u}_B^{n+1} = \{u_{j,k}^{n+1} | (j,k) \in I_B\}$ on the boundaries. Combine the numerical solution $\mathbf{u}_B^{n+1}$ and the numerical solution $\mathbf{u}_I^{n+1}$ obtained by solving Eq. (3.1), one gets the numerical solution $\mathbf{u}^{n+1}$ at time $t = t_{n+1}$.

So far, the simple operator splitting method has been described. In order to improve the accuracy, the Strang splitting method [29] can be used, where we introduce two intermediate variables

$$U^* = \left\{ [u_{jk}^*, v_{jk}^*]^T | (j,k) \in I_B \right\} \quad \text{and} \quad U^{**} = \left\{ [u_{jk}^{**}, v_{jk}^{**}]^T | (j,k) \in I_B \right\}.$$

Here U^* is obtained from U^n through the half time step of the nonlinear subproblem (2.4a)-(2.4b) on the boundaries,

$$U^* \approx \mathcal{F}_2^{\frac{\tau}{2}}(U^n), \quad (j,k) \in I_B. \tag{3.5}$$

Suppose that $v_{jk}^{**} = v_{jk}^*$, $(j,k) \in I_B$. And u_{jk}^{**}, $(j,k) \in I_B$ are obtained from the boundary condition equations (3.2)-(3.3c) by replacing u_{jk}^n with u_{jk}^* and u_{jk}^{n+1} with u_{jk}^{**}, respectively. Finally, U_B^{n+1} is obtained from U^{**} through another half time step of the nonlinear subproblem (2.4a)-(2.4b) on the boundaries,

$$U_B^{n+1} \approx \mathcal{F}_2^{\frac{\tau}{2}}(U^{**}), \quad (j,k) \in I_B. \tag{3.6}$$

The component $\mathbf{u}_B^{n+1}$ in U_B^{n+1} is the numerical solution on the boundaries at time $t = t_{n+1}$, and the component $\mathbf{v}_B^{n+1}$ will be recorded for the next time step.

4 Numerical results

In this section we present numerical examples to demonstrate the validity of the proposed split local artificial boundary conditions for the two-dimensional sine-Gordon problem (1.1a)-(1.1b) on R^2 and to show the numerical accuracy of the numerical scheme. We choose the initial data the same as those in [7, 8, 10, 11], which are called *line* and *ring solitons*.

The choice of the splitting control parameter α is quite important in the proposed method, however how to get the α in an analytic way is still open. Through numerical experiment, we find that a larger α will have a better performance for the split local

ABC. Therefore we choose $\alpha = 0.9$ in the numerical test. The choices of the integer p and the angles θ_l, $l = 1,\cdots,p$ in the boundary conditions (2.14)-(2.15c) are also important. In [26–28], Higdon studied the relation between the amplitude of the reflected waves and the parameter p and θ_l, $l = 1,\cdots,p$. Through numerical experiments, we find that one simply chooses $p = 2$ and $\theta_1 = \theta_2 = 0$, the given method is nearly transparent for the wave propagation. However, how to adaptively choose the optimal p and θ_l, $l = 1,\cdots,p$ to reduce the amplitude of the reflected waves is still open and will be our further consideration.

4.1 Soliton-type solutions of the sine-Gordon equation

The sine-Gordon equation allows for solitary wave solutions, a ubiquitous phenomenon in a large variety of physical problem. In this subsection, we use the proposed split local artificial conditions to solve the two-dimensional sine-Gordon problem on R^2 and investigate the corresponding solitary wave solutions. Our numerical experiments are carried out for the following cases: (1) Superposition of two orthogonal line solitons; (2) Symmetric perturbation of a static line solitons; (3) Circular ring solitons; (4) Elliptical breather; (5) Collision of four circular solitons. The first two are typical *line solitons*, and the rest three are typical *ring solitons*.

The energy conservation of the sine-Gordon equation (1.1a) has been proven to be a characteristic property of the nonlinear solitary waves. In this section, we define the energy of the sine-Gordon equation (1.1a) on the bounded domain D_i by the following expression:

$$E(t) = \frac{1}{2}\int_{x_w}^{x_e}\int_{y_s}^{y_n}\Big(u_t^2 + u_x^2 + u_y^2 + 2(1-\cos u)\Big)dxdy. \tag{4.1}$$

The energy $E(t)$ can be calculated numerically through the numerical quadrature to approximate Eq. (4.1). Our concern is with the dynamic behaviors of the different solitary wave solutions and the energy conservation property of the solitary waves. In all of the experiments in this subsection, except when otherwise defined, $h_x = h_y = h = 1/16$ and $\tau = 1/32$ are used.

4.1.1 Superposition of two orthogonal line solitons

As considered in [2], if one line soliton operates along the x-axis and the other on the y-axis, an exact solution to the sine-Gordon equation can be obtained. Soliton solution to the sine-Gordon equation (1.1a) with initial conditions

$$\begin{aligned}
&\varphi_0(x,y) = 4\big(\tan^{-1}(e^x) + \tan^{-1}(e^y)\big), && x,y \in \mathrm{R}^1,\\
&\varphi_1(x,y) = 0, && x,y \in \mathrm{R}^1,
\end{aligned}$$

is called the *superposition of two orthogonal line solitons* in the literature, see [9, 11]. In this example, the bounded computational domain is chosen to be $[-6,6]\times[-6,6]$. In Fig. 1,

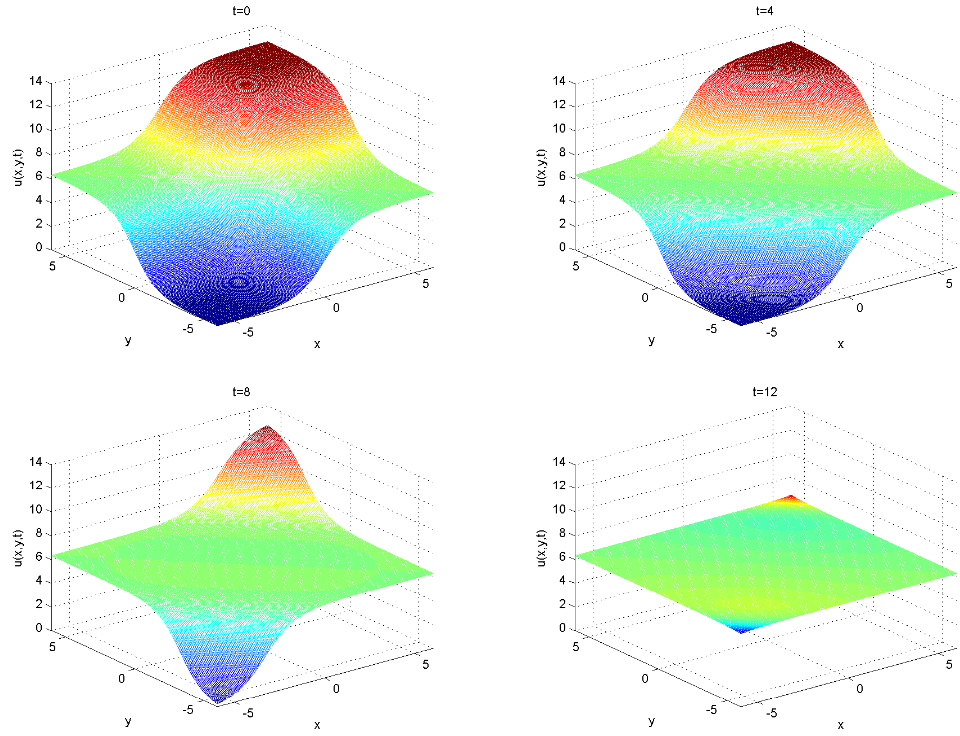

Figure 1: Superposition of two orthogonal line solitons at time $t=0,4,8,12$.

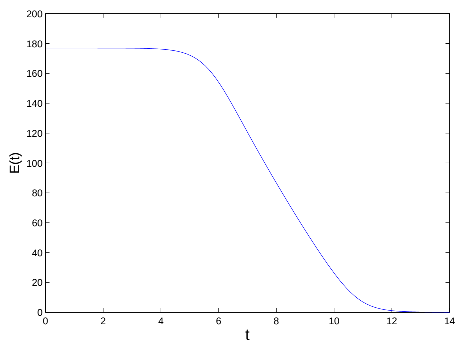

Figure 2: The energy of the superposition of two orthogonal line solitons.

we present the snapshots of the numerical solution at several different times. The initial data is the superposition of two orthogonal line solitons along the x-direction and the y-direction. Then they move away from each other in the direction of $y=x$, finally the solitons travel out the computational domain with negligible reflection, which shows that the proposed boundary conditions are nearly transparent for the wave propagation. In Fig. 2, we plot the energy of the solitons remaining in the bounded domain. As the solitons move away from the bounded domain, the energy gradually decays to zero.

4.1.2 Symmetric perturbation of a static line soliton

A static line soliton is perturbed to produce two symmetric dents moving towards each other with a constant velocity is called *symmetric perturbation of a static line soliton*. According to [2], the dents collide and continue to move with the same velocity and no shift occurs. In this case, the initial data of the sine-Gordon equation (1.1a) is defined by:

$$\varphi_0(x,y)=4\tan^{-1}\exp\left(x+1-\frac{2}{\cosh(y+7)}-\frac{2}{\cosh(y-7)}\right),\quad x,y\in\mathrm{R}^1,$$
$$\varphi_1(x,y)=0,\qquad x,y\in\mathrm{R}^1.$$

In this example, the bounded computational domain is chosen to be $[-7,7]\times[-7,7]$.

Fig. 3 depicts the snapshots of the numerical solutions in terms of $\sin(u/2)$ at different times. At time $t=0$, the initial wave displacement of the symmetric perturbation of a static line soliton is shown. Then at time $t=3$, one can see that the perturbation move toward to each other. We point out that part of perturbation has moved out the bounded computational domain, which can be verified by the energy decreasing in Fig. 4. Around time $t=7$ the two symmetric dents move close to each other and collide. Compare the solution at time $t=11$ with that at time $t=3$, one can see that after the collision, the two

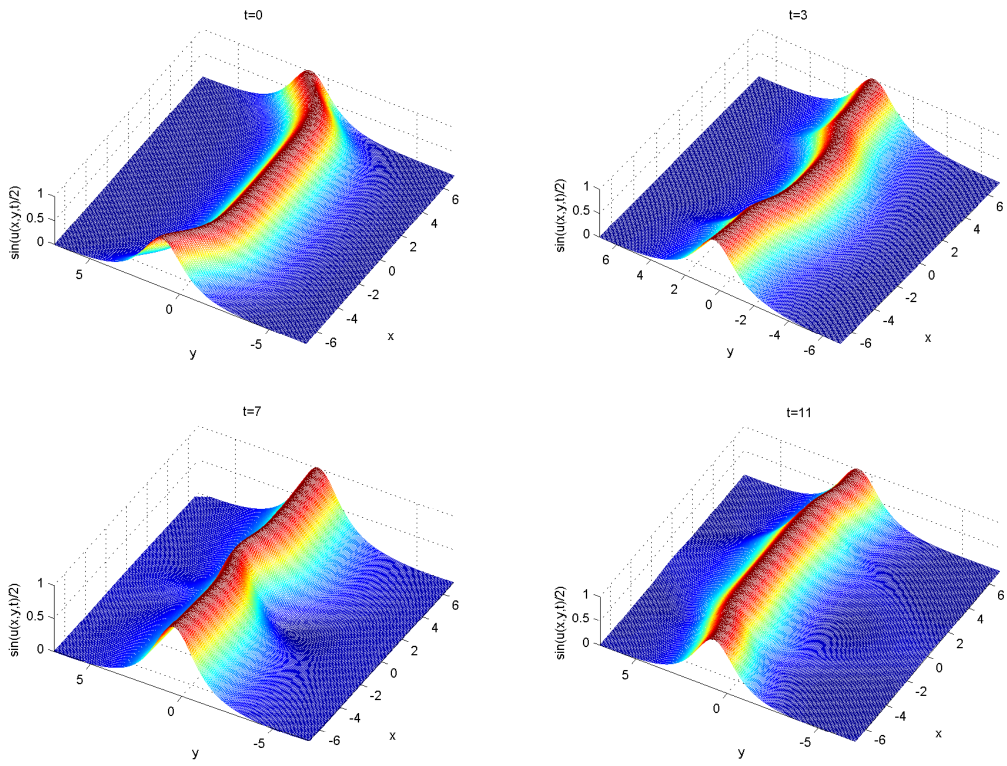

Figure 3: Symmetric perturbation of a static line soliton at time $t=0,3,7,11$.

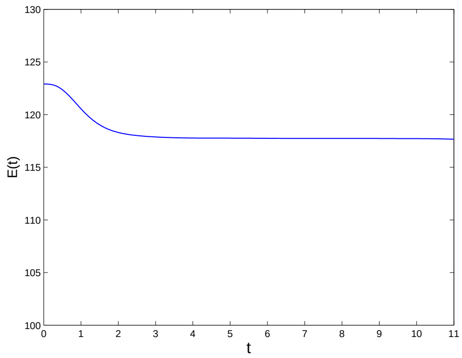

Figure 4: The energy of the symmetric perturbation of a static line soliton.

symmetric dents continue to move with the same velocity and retain their shapes. Fig. 4 also indicates that when the part of the perturbation wave move out of the bounded computational domain, the remaining energy is conserved.

4.1.3 Circular ring solitons

The two-dimensional sine-Gordon equation also admits the ring soliton solutions. In [2, 3], the authors investigated the pulsating behaviors of the *circular ring soliton* solutions. The initial condition of the circular ring soliton is given by:

$$\begin{aligned} &\varphi_0(x,y)=4\tan^{-1}\exp\left(3-\sqrt{x^2+y^2}\right), && x,y\in\mathrm{R}^1,\\ &\varphi_1(x,y)=0, && x,y\in\mathrm{R}^1. \end{aligned}$$

In this example, the bounded computational domain is chosen to be $[-7,7]\times[-7,7]$.

In Fig. 5 and Fig. 6, we present the snapshots of the numerical solution in term of $\sin(u/2)$ at several different times. Initially at time $t=0$, the soliton appears as two homocentric rings, then as time goes on, at time $t=3$, the soliton shrinks and appears like a single ring soliton. At time $t=6$, which could be considered as the beginning of the expansion, a radiation appears, which is followed by oscillations at the boundaries, as shown at time $t=9$. This expansion is continued until at time $t=11$, when in the center part of the domain, the soliton is almost restored. Finally from $t=13$, it appears to be in its shrinking process again. During the whole evolution process, the center of the circular ring soliton does not move.

Fig. 7 shows that before time $t=9$ the energy is conserved, since the movement of circular ring soliton is restricted in the bounded domain, however after time $t=9$ as the radiation process goes on, the circular ring soliton moves out the bounded domain and the energy decays accordingly.

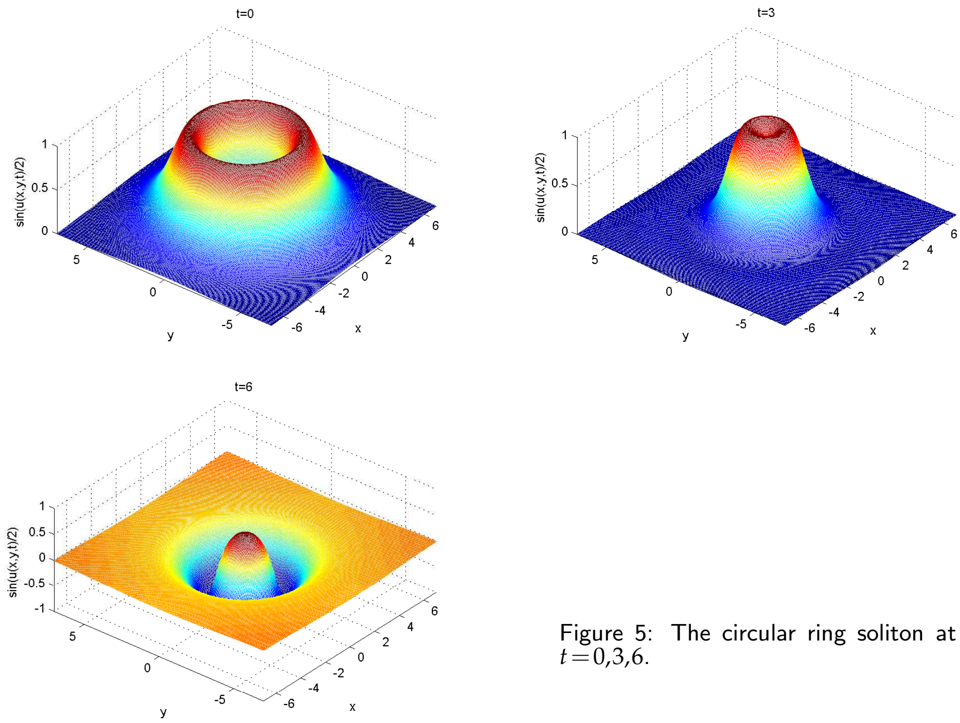

Figure 5: The circular ring soliton at time $t=0,3,6$.

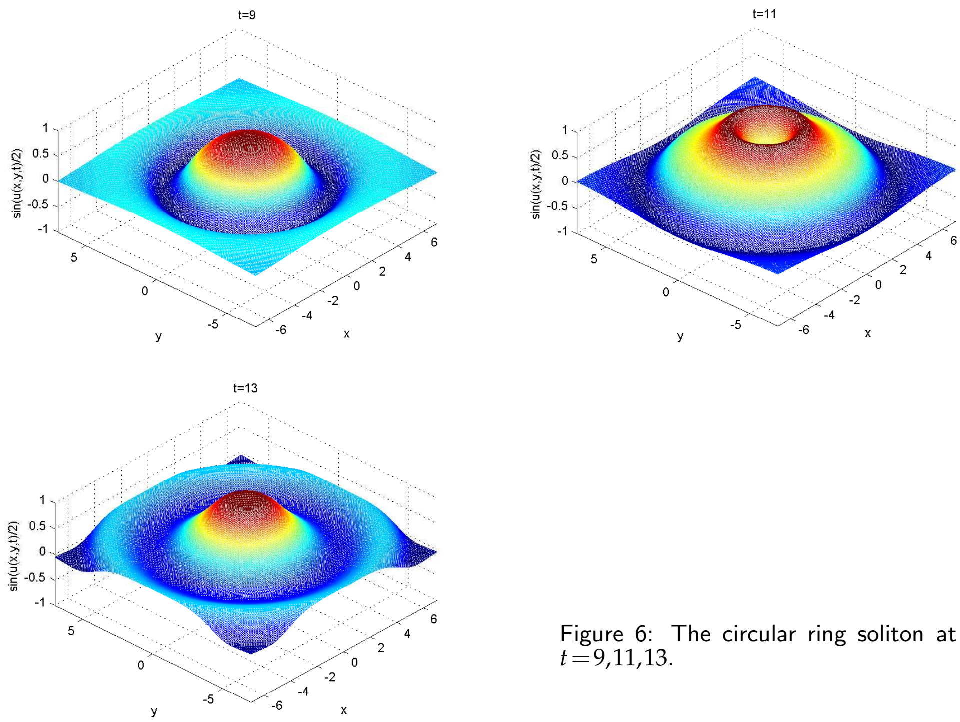

Figure 6: The circular ring soliton at time $t=9,11,13$.

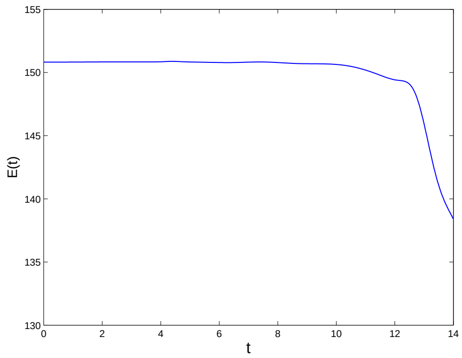

Figure 7: The energy of the circular ring soliton.

4.1.4 Elliptical breather

The *elliptical breather* is another kind of ring soliton solution to the two-dimensional sine-Gordon equation, see [11]. The initial condition of the elliptical breather is given by:

$$
\begin{aligned}
&\varphi_0(x,y)=4\tan^{-1}\frac{2}{\cosh\left(0.866\sqrt{\frac{(x-y)^2}{3}+\frac{(x+y)^2}{2}}\right)}, && x,y\in\mathrm{R}^1,\\
&\varphi_1(x,y)=0, && x,y\in\mathrm{R}^1.
\end{aligned}
$$

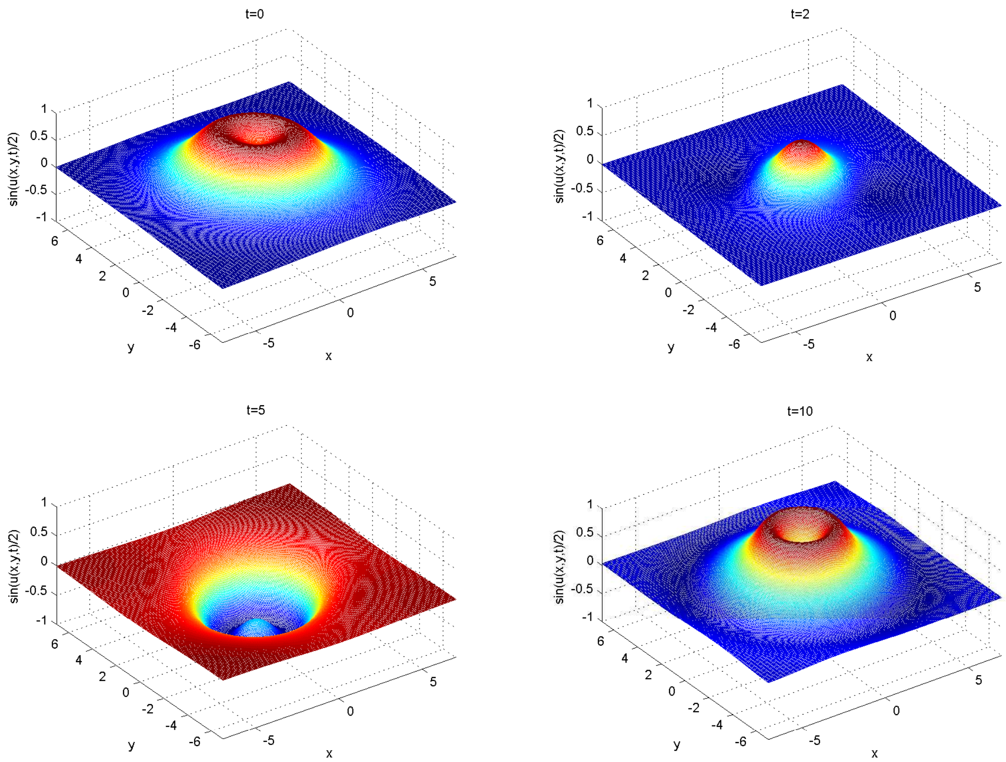

Figure 8: Elliptical breather at time $t=0,2,5,10$.

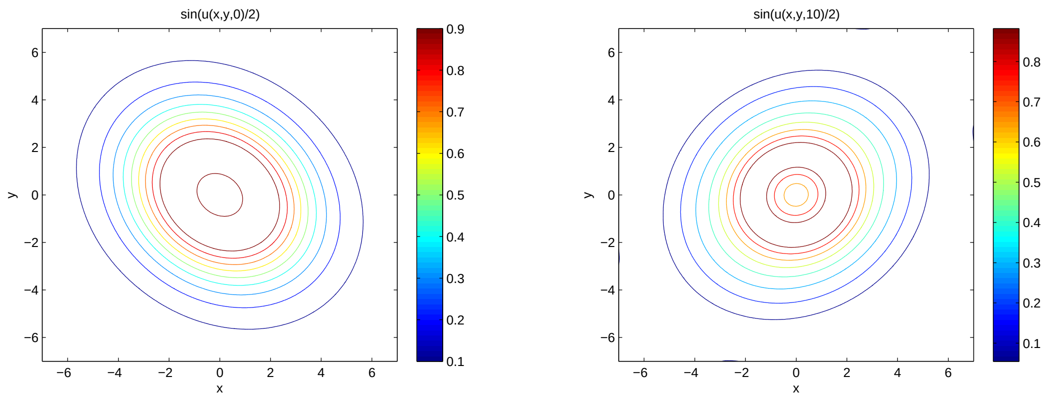

Figure 9: The contours of the elliptical breather. The left is at time $t=0$ and the right is at time $t=10$.

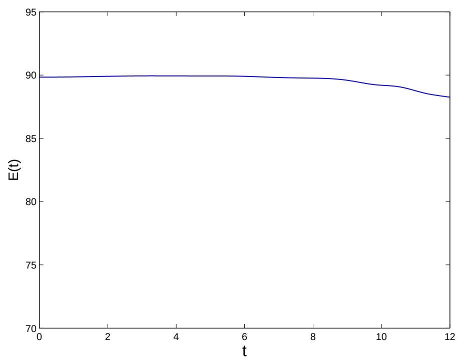

Figure 10: The energy of the elliptical breather.

In this example, the bounded computational domain is chosen to be $[-7,7]\times[-7,7]$.

In Fig. 8, we present the snapshots of the numerical solution of the elliptical breather in term of $\sin(u/2)$ at several different times. The major axis of the breather from its initial direction $y=-x$ seems to be turned clockwise. The same as the *circular ring solitons*, the shrinking and expansion process are observed from time $t=2$ to $t=10$. Around time $t=10$, the elliptical breather seems to recover its initial shape, however the major axis changes to $y=x$, which is verified in the contour plot in Fig. 9. From time $t=10$ when the second shrinking process begins, part of the solitary wave will move out of the bounded computational domain, hence the energy plot begins to decay, which has been shown in Fig. 10.

4.1.5 Collision of four expanding circular solitons

Finally, we observe an interesting phenomena of the solitary solution to the two-dimensional sine-Gordon equation, namely, the *collision of four expanding circular solitons*.

First of all, we introduce some function notations. Let

$$\phi_0(x,y;x_0,y_0)=4\tan^{-1}\exp\left[\frac{1}{0.436}\left(4-\sqrt{(x+x_0^2)+(y+y_0)^2}\right)\right],\quad x,y\in\mathrm{R}^1,$$

denote the initial displacement of a circular ring soliton centered at the point (x_0,y_0), and the corresponding initial velocity is given by

$$\phi_1(x,y;x_0,y_0)=4.13\left[\cosh\left(\frac{1}{0.436}\left(4-\sqrt{(x+x_0^2)+(y+y_0)^2}\right)\right)\right]^{-1},\quad x,y\in\mathrm{R}^1.$$

Then the initial conditions of the collision of four expanding circular ring solitons are given by,

$$\varphi_0(x,y)=\phi_0(x,y;5,5)+\phi_0(x,y;5,-5)+\phi_0(x,y;-5,5)+\phi_0(x,y;-5,-5),\quad x,y\in\mathrm{R}^1,$$
$$\varphi_1(x,y)=\phi_1(x,y;5,5)+\phi_1(x,y;5,-5)+\phi_1(x,y;-5,5)+\phi_1(x,y;-5,-5),\quad x,y\in\mathrm{R}^1,$$

which are the superposition of four circular ring solitons.

In this example, the bounded computational domain is chosen to be $[-12,12]\times[-12,12]$.

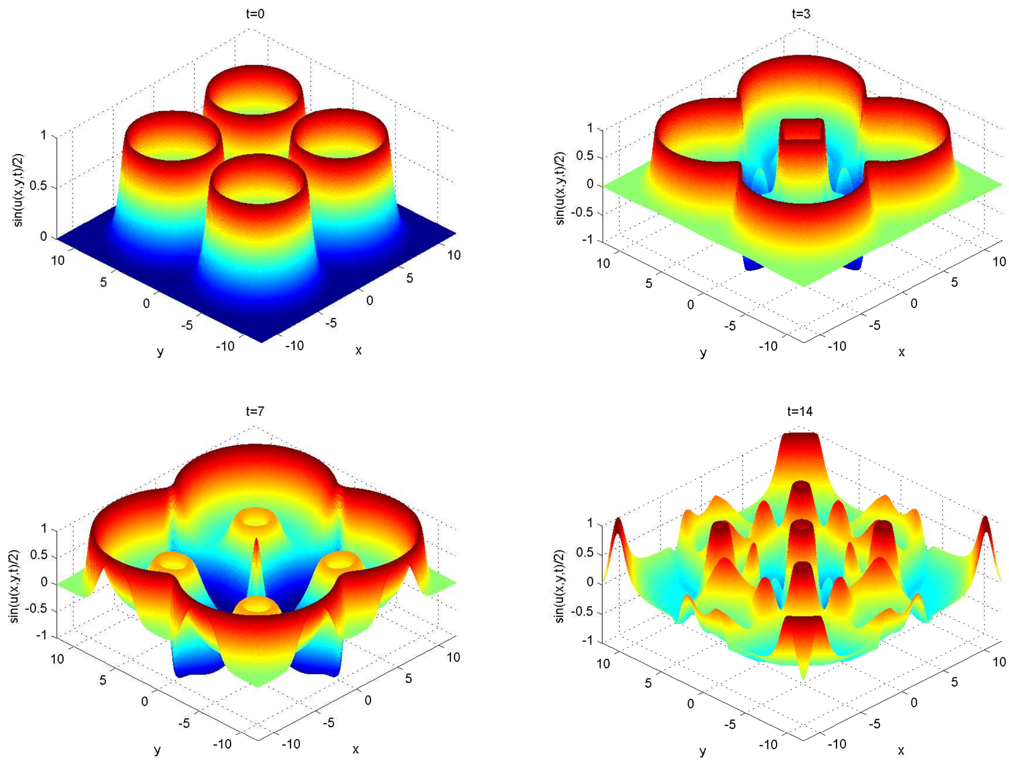

Figure 11: The collision of four expanding circular solitons at time $t=0,3,7,14$.

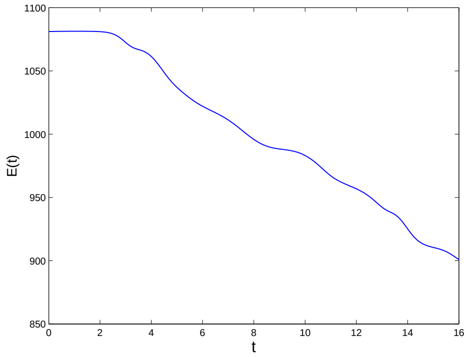

Figure 12: The energy of the collision of four expanding circular solitons.

In Fig. 11, we present the snapshots of the numerical solution in term of $\sin(u/2)$ at several different times. Initially, at time $t=0$ four circular ring solitons are isolated from each other on the bounded domain. Then they expand quickly, collide with each other and move out of the bounded domain. Then at time $t=3$, $t=7$ and $t=14$, respectively, we give the snapshots of this interesting phenomena obtained by our proposed method.

Fig. 12 shows that before time $t=3$ the energy is conserved, since the movement of circular ring solitons are restricted in the bounded domain, however after time t=3 as the circular ring solitons move out the bounded domain and the energy decays accordingly.

4.2 Accuracy of the proposed method

In this section, we consider the numerical accuracy of the proposed method for the sine-Gordon equation. Numerical experiments show that for these solitary solutions to the two-dimensional sine-Gordon equation, the proposed method has the same accuracy. To avoid tautology, we only choose some results in the line soliton and ring soliton as example. In the computations, we set $\tau=h/2$. To evaluate the accuracy of numerical solution, we define the error functions as following

$$
\begin{aligned}
&Error_\infty(t)=\max|u_{exa}(\cdot,\cdot,t)-u_{num}(\cdot,\cdot,t)|,\\
&Error_1(t)=\|u_{exa}(\cdot,\cdot,t)-u_{num}(\cdot,\cdot,t)\|_{L_1},\\
&Error_2(t)=\|u_{exa}(\cdot,\cdot,t)-u_{num}(\cdot,\cdot,t)\|_{L_2}.
\end{aligned}
$$

Tables 1 and 2 list the corresponding errors for the *superposition of two orthogonal line solitons* and the *collision of four circular solitons* at time $t=8$, respectively. The same as the previous section, the bounded spatial computational domain is chosen to be $[-6,6]\times[-6,6]$ for the *superposition of two orthogonal line solitons* and $[-12,12]\times[-12,12]$ for the *collision of four circular solitons*.

Fig. 13 shows that when we vary the mesh size $h=1/4$, $1/8$, $1/16$, $1/32$, $1/64$, the error functions $Error_\infty$, $Error_1$ and $Error_2$ converge. The reference solution $u(\cdot,\cdot,t)_{exa}$ for

Table 1: The errors for the superposition of two orthogonal line solitons at time $t=8$.

Mesh	$Error_\infty(8)$	$Error_1(8)$	$Error_2(8)$
$h=\frac{1}{4}$	1.7854e-1	5.2452e-0	7.2354e-1
$h=\frac{1}{8}$	7.5990e-2	2.2464e-0	3.1367e-1
$h=\frac{1}{16}$	3.3188e-2	9.8453e-1	1.3832e-1
$h=\frac{1}{32}$	1.3760e-2	4.0868e-1	5.7596e-2
$h=\frac{1}{64}$	4.5127e-3	1.3405e-1	1.8921e-2

Table 2: The errors for the collision of four circular solitons at time $t=8$.

Mesh	$Error_\infty(8)$	$Error_1(8)$	$Error_2(8)$
$h=\frac{1}{4}$	2.8463e-1	4.2045e1	2.2075e0
$h=\frac{1}{8}$	1.3413e-1	1.9353e1	1.0061e0
$h=\frac{1}{16}$	6.4796e-2	8.8584e0	4.6075e-1
$h=\frac{1}{32}$	2.8301e-2	3.7682e0	1.9643e-1
$h=\frac{1}{64}$	9.5293e-3	1.2522e0	6.5379e-2

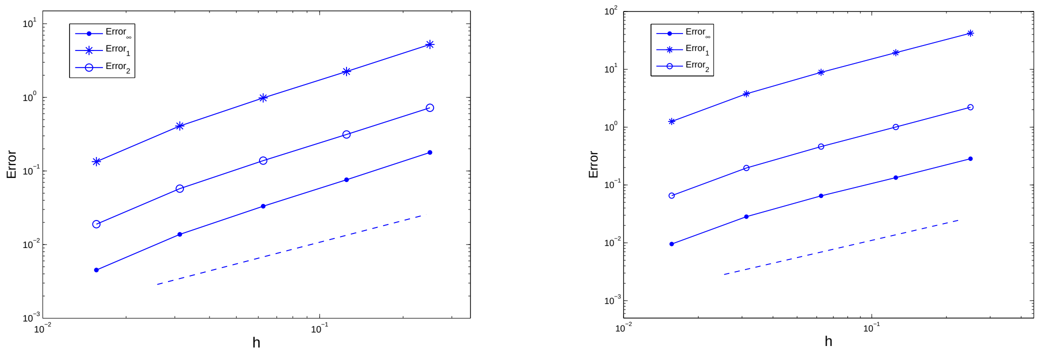

Figure 13: The errors of the proposed method at time $t=8$, when varying the mesh size $h=1/4,1/8,1/16,1/32,1/64$. The left is for the *superposition of two orthogonal line solitons* and the right is for the *collision of four circular solitons*. The dashed lines converge in the order $\mathcal{O}(h)$.

the *superposition of two orthogonal line solitons* (*collision of four circular solitons*) is obtained on the bounded spatial domain $[-10,10]\times[-10,10]$ ($[-18,18]\times[-18,18]$) with the mesh size $h=1/128$. These bounded spatial domains are large enough, so that during all the computational times, the waves do not touch the boundaries.

The choice of the splitting control parameter α is quite important in the split local artificial boundary conditions method, however how to get the α in an analytic way is still open. Through numerical experiments, we find that a larger α will have a better performance for the split local ABC. Fig. 14 gives the numerical errors of different splitting control parameter α for the *circular ring solitons* at time $t=8$. Here the error function is defined by the L_1 norm, with mesh size $h=1/16$ and $h=1/32$ respectively.

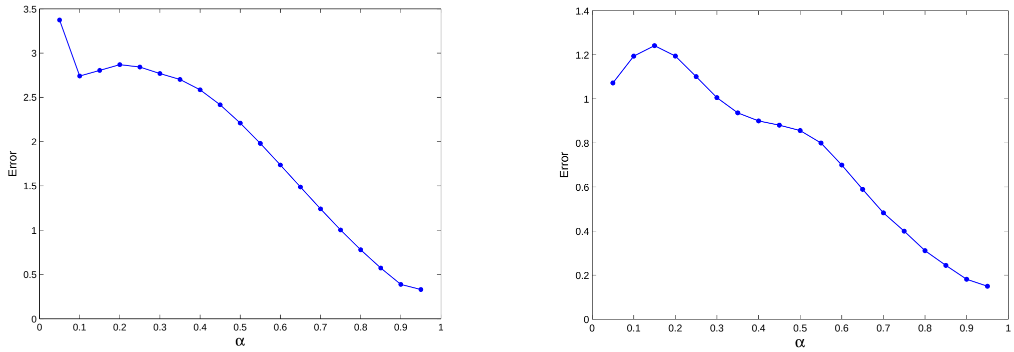

Figure 14: The errors of different splitting control parameter α for the *circular ring soliton* at $t=8$. Left is $h=1/16$, right is $h=1/32$. $\tau=h/2$.

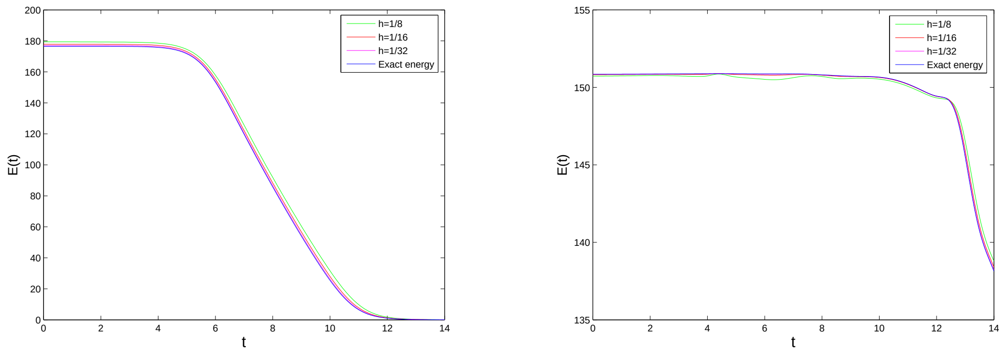

Figure 15: The energy decays of different mesh size. The left is for the *superposition of two orthogonal line solitons* and the right is for the *circular ring solitons*. The exact energy is obtained on the mesh size $h=1/128$.

The energy conservation of the sine-Gordon equation has been proven to be a characteristic property of the nonlinear solitary waves. Fig. 15 plots the energy decaying on the bounded domain between the numerical solution and the "exact" solution for the purpose of comparison. The "exact" solution is obtained on the mesh size $h=1/128$.

5 Conclusions

The numerical solution to the two-dimensional sine-Gordon equation on R^2 is studied in this paper. Split local artificial boundary conditions are obtained by the operator splitting method, then the original initial value problem is reduced to an initial boundary value problem on a bounded computational domain. Numerical examples about the propagation and collision of solitary wave solutions are tested, which indicates that the proposed split local artificial boundary conditions are nearly transparent for the wave propagation.

The proposed artificial boundary conditions are valid under the assumptions that during the propagation process only the waves in the interior domain will move out of the domain through the artificial boundaries and there will be no waves traveling from the exterior domain into the interior domain. For general cases, where both the outgoing and in-going waves travel through the artificial boundaries, the artificial boundary conditions are complicated and will be our further consideration.

Acknowledgments

The authors would like to thank the financial support form the National Natural Science Foundation of China (Grant No. 10971116).

References

[1] J. D. Josephson, Supercurrents through barriers, Adv. Phys., 14 (1965), 419–451.
[2] P. L. Christiansen and P. S. Lomdahl, Numerical solution of 2+1 dimensional sine-Gordon solitons, Phys. D, 2 (1981), 482–494.
[3] I. L. Bogolyubski and V. G. Makhankov, Lifetime of pulsating solitons in certain classical models, JETP Lett., 24(1) (1976), 12–14.
[4] H. Han, The Artifial Boundary Method-Numerical Solutions of Partial Differential Equations on Unbounded Domains, Frontier and Prospects of Comtemporary Applied Mathematics, 2005, Higher Education Press, World Scientific.
[5] B.-Y. Guo, P. J. Pascual, M. J. Rodriguez and L. Vazquez, Numerical solution of the sine-Gordon equation, Appl. Math. Comput., 18 (1986), 1–14.
[6] J. X. Xin, Modeling light bullets with the two-dimensional sine-Gordon equation, Phys. D, 135 (2000), 345–368.
[7] P. L. Christiansen and P. S. Lomdahl, Numerical solutions of 2+1 dimensional sine-Gordon solitons, Phys. D, 2 (1981), 482–494.
[8] J. Argyris, M. Haase and J. C. Heinrich, Finite element approximation to two-dimensional sine-Gordon solitons, Comput. Methods Appl. Mech. Eng., 86 (1991), 1–26.
[9] Q. Sheng, A. Q. M. Khaliq and D. A. Voss, Numerical simulation of two-dimensional sine-Gordon solitons via a split cosine scheme, Math. Comput. Sim., 68 (2005), 355–373.
[10] K. Djidjeli, W. G. Price and E. H. Twizell, Numerical solutions of a damped sine-Gordon equation in two space variables, J. Eng. Math., 29 (1995), 347–369.
[11] A. G. Bratsos, An explicit numerical scheme for the sine-Gordon equation in 2+1 dimensions, Appl. Numer. Anal. Comput. Math., 2(2) (2005), 189–211.
[12] A. G. Bratsos, The solution of the two-dimensional sine-Gordon equation using the method of lines, J. Comput. Appl. Math., 206 (2007), 251–277.
[13] M. Dehghan and A. Shokri, A numerical method for solution of the two-dimensional sine-Gordon equation using the radial basis functions, Math. Comput. Sim., 79 (2008), 700–715.
[14] D. Mirzaei and M. Dehghan, Boundary element solution of the two-dimensional sine-Gordonequation using continuous linear elements, Eng. Anal. Bound. Elem., 33 (2009), 12–24.
[15] B. Engquist and A. Majda, Absorbing boundary conditions for the numerical simulation of waves, Math. Comput., 31 (1986), 629–651.
[16] D. Givoli, High-order local non-reflecting boundary conditions: a review, Wave Motion, 39 (2004), 319–326.

[17] T. Hagstrom, Radiation boundary conditions for the numerical simulation of waves, Acta. Number., 8 (1999), 47–106.
[18] M. J. Grote and J. B. Keller, Exact non-reflecting boundary conditions for the time dependent wave equation, SIAM J. Appl. Math., 55(2) (1995), 280–297.
[19] H. Han and C. Zheng, Exact non-reflecting boundary conditions for an acoustic problem in three dimensions, J. Comput. Math., 21(1) (2003), 15–24.
[20] H. Han, X. Wu and Z. Xu, Artificial boundary method for Burger's equation using nonlinear boundary conditions, J. Comput. Math., 24 (2006), 295–304.
[21] Z. Xu, H. Han and X. Wu, Numerical method for the determimistic Kardar-Parisi-Zhang equation in unbounded domians, Commun. Comput. Phys., 1 (2006), 479–493.
[22] H. Han and Z. W. Zhang, Split local absorbing conditions for one-dimensional nonlinear Klein-Gordon equation on unbounded domain, J. Comput. Phys., 227 (2008), 8992–9004.
[23] C. Zheng, Exact nonreflection boundary conditions for one-dimensional cubic nonlinear Schrödinger equations, J. Comput. Phys., 215 (2006), 552–565.
[24] C. Zheng, Numerical solution to the sine-Gordon equation defined on the whole real axis, SIAM J. Sci. Comput., 29(6) (2007), 2494–2506.
[25] B. Engquist and A. Majda, Radiation boundary conditions for acoustic and elastic wave calculations, Commun. Pure Appl. Math., 32 (1979), 314–358.
[26] R. L. Higdon, Absorbing boundary conditions for difference approximations to the multi-dimensional wave equation, Math. Comput., 47 (1986), 437–459.
[27] R. L. Higdon, Numerical absorbing boundary conditions for the wave equation, Math. Comput., 49 (1987), 65–90.
[28] R. L. Higdon, Radiation boundary conditions for dispersive waves, SIAM J. Numer. Anal., 31 (1994), 64–100.
[29] G. Strang, On the construction and comparison of difference schemes, SIAM J. Numer. Anal., 5 (1968), 506–517.
[30] S. Yu, S. Zhao and G. W. Wei, Local spectral time splitting method for first- and second-order partial differential equations, J. Comput. Phys., 206 (2005), 727–780.